

Effect of europium concentration on photoluminescence and thermoluminescence behavior of $Y_2O_3:Eu^{3+}$ phosphor

Vikas Dubey · Jagjeet Kaur · Sadhana Agrawal

Received: 17 November 2013 / Accepted: 12 February 2014 / Published online: 4 March 2014
© Springer Science+Business Media Dordrecht 2014

Abstract The present paper reports the synthesis, photoluminescence (PL), and thermoluminescence (TL) studies of Eu^{3+} -doped yttrium oxide (Y_2O_3) phosphor using inorganic materials like Y_2O_3 , flux calcium fluoride, and europium oxide. The sample was prepared by the modified solid state reaction method, which is the most suitable for large-scale production. The prepared phosphor sample was characterized using powder X-ray diffraction, field emission gun scanning electron microscopy, high resolution transmission electron microscopy, Fourier transform infrared spectroscopy, PL, TL, and Commission Internationale de l'Eclairage techniques. The PL emission was observed in the range 417–632 nm ranges all visible regions for the Y_2O_3 phosphor doped with Eu^{3+} . Excitation spectrum found at 254 nm. Sharp intense peaks found around 467, 534, 594, 612, and 632 nm with high intensity. From the XRD data, using the Scherer's formula, the calculated average crystallite size of Eu^{3+} -doped Y_2O_3 phosphor is around 45 nm. TL study was carried out for the phosphor with UV irradiation. The present phosphor can act as single host for white light emission in display devices.

Keywords Photoluminescence (PL) · Thermoluminescence (TL) · XRD · SEM · CIE

V. Dubey (✉)
Bhilai Institute of Technology, Kendri, Raipur, C.G., India
e-mail: jsvikasdubey@gmail.com

V. Dubey · S. Agrawal
Department of Physics, National Institute of Technology, Raipur, C.G., India

J. Kaur
Department of Physics, Govt. Vishwanath Yadav Tamaskar Post Graduate Autonomous College,
Durg 491001, C.G., India

Introduction

Rare earth sesquioxides (RE_2O_3) have been of great scientific and technological interest for many years because of their attractive physical and chemical properties. Actually, they are excellent host materials for lasers, with high thermal stability [1–3]. Yttrium oxide (Y_2O_3), for example, is an interesting host material for high power laser applications with a very high melting point of $\sim 2,430^\circ\text{C}$, a cubic structure of the space group $\text{Ia}\bar{3}$, and a lattice constant of 10.6041 \AA [4, 5]. Numerous studies have been carried out on the synthesis and properties of rare earth-doped Y_2O_3 [6–9]. Y_2O_3 seems to be an ideal matrix as it is a chemically very stable, high band gap (5.6 eV), transparent host with a low phonon energy ($\sim 430\text{--}550 \text{ cm}^{-1}$), etc. [10]. Beside this, the ionic radius of Y^{3+} is almost similar to the other trivalent RE ions (RE^{3+}), and so, by Shannon effective ionic radius theory [11], it can be easily and effectively doped with RE^{3+} ions. The RE^{3+} ions attach at a suitable site in the matrix and interact with the field of host lattice giving rise to a characteristic strong, sharp, and Stark splitted visible emission bands of RE^{3+} ions. $\text{Y}_2\text{O}_3:\text{Eu}^{3+}$ phosphor emits red emissions and has excellent chemical stability. This phosphor is the only existing red phosphor used in three-band fluorescent lamps (FL). The luminescence property of the phosphors is very much dependent on the synthesis route that has been adopted. $\text{Y}_2\text{O}_3:\text{Eu}$ phosphor has been synthesized by conventional solid-state synthesis [12].

Y_2O_3 is known as a very important material owing to its chemical and physical unique property, which has been used and also shows versatile potential applications in broad fields, such as transparent ceramics [13], catalysts [14], sensors [15], and biological labels [16]. In particular, Y_2O_3 - and Y_2O_3 -doped transparent ceramics are outstanding opto functional materials and have been widely studied as promising materials for laser ceramics [17, 18] and scintillation ceramics [19]. As is well known, morphology and size of nano- or micro-scale materials have great influence on their properties [20] as well as reactivity when preparing bulk materials such as transparent ceramics. Therefore, it is very important to synthesize powder materials with controllable morphology so as to control the reaction procedure and production quality of the bulk material. During the last several decades, various methods have been attempted to the morphology-controllable fabrications of Y_2O_3 - or Y_2O_3 -doped materials with certain size and shape to improve its properties and then to explore its multifunctional applications [21–28].

The rare-earth ions show abundant emission colors based on their $4f\text{--}4f$ or $5d\text{--}4f$ transitions. Eu^{3+} shows red/orange emission, while $\text{Y}_2\text{O}_3:\text{Eu}^{3+}$ phosphor shows a red emission and has excellent chemical stability. This phosphor is the only existing red/green phosphor used in three-band FL. For $\text{Y}_2\text{O}_3:\text{Eu}$ nanoparticles, the intensity of $^5\text{D}_1$ emission of Eu^{3+} ions from the C3i site (S6) is significantly less compared to the emission of Eu^{3+} ions in the C_2 site for these samples [29]. The Eu–O charge transfer band (CTB) resulting from an electron transfer from the ligand O^{2-} (2p) orbit to the empty states of the $4f^6$ configuration ($\text{Eu}^{3+}\text{--}\text{O}^{2-}$ transition) and the energy transfer efficiency between the Y_2O_3 host and Eu^{3+} ions were investigated by Kelley et al. [30].

$\text{Y}_2\text{O}_3:\text{Eu}^{3+}$ phosphor exhibits red emissions and has excellent chemical stability. This phosphor is the only existing red phosphor used in three-band FL [9]. $\text{Y}_2\text{O}_3:\text{Eu}^{3+}$ has attracted a great deal of interest for use as red phosphor in FL, high-resolution

projection TVs, protection devices, and low voltage displays such as cathode ray tubes, plasma display panels, and field emission displays [31, 32]. Recent studies on different luminescent nanomaterials have shown a potential application in dosimetry of ionizing radiations for the measurement of high doses using the TL technique [33]. Y_2O_3 doped with trivalent rare earth ions is a well-known material for display and lamp applications. And such materials may be investigated for their potential application as TL dosimeters or scintillating detectors [34].

In this paper, the solid state reaction method was used to synthesize $Y_2O_3:Eu^{3+}$ phosphor. It is suitable for large-scale production. Samples were characterized by different techniques such as XRD, field emission gun scanning electron microscopy (FEGSEM), high resolution transmission electron microscopy (HRTEM), Fourier transform infrared spectroscopy (FTIR), PL, and TL studies. The effect of Eu^{3+} concentration on PL and TL studies are also interpreted.

Experimental

Preparation of Y_2O_3 with europium (0.1–2.5 mol%) consists of heating stoichiometric amounts of reactant mixture in an alumina crucible fired in air at 1,300 °C for 4 h in a muffle furnace. Every heating is followed by intermediate grinding using an agate mortar and pestle. The Eu-activated Y_2O_3 phosphor was prepared via a high temperature solid state method. The starting materials were as follows: Y_2O_3 , europium oxide (Eu_2O_3) and CaF_2 (as a flux) in molar ratio were used to prepare the phosphor [35].

The sample was characterized using photoluminescence (PL), thermoluminescence (TL), XRD, FEGSEM, and HRTEM. The XRD measurements were carried out using a Bruker D8 Advance X-ray diffractometer. The X-rays were produced using a sealed tube and the wavelength of X-ray was 0.154 nm ($Cu K\alpha$). The X-rays were detected using a fast counting detector based on silicon strip technology (Bruker Lynx Eye detector). Observation of particle morphology was investigated by FEGSEM (JEOL JSM-6360). FTIR spectra were recorded using a 3000 Hyperion Microscope with Vertex 80 FTIR System; Bruker, Germany). The PL emission and excitation spectra were recorded at room temperature by use of a Shimadzu RF-5301 PC spectrofluorophotometer. The excitation source was a xenon lamp. Thermally stimulated luminescence glow curves were recorded at room temperature by using TLD reader I1009 supplied by Nucleonix, Hyderabad. The obtained phosphor under the TL examination was given UV radiation using a 254-nm UV source [35–39].

Results and discussion

Figure 1 shows the X-ray powder diffraction (XRD) pattern of $Y_2O_3:Eu^{3+}$ (0.5–2.5 mol% of Eu) phosphor. From the XRD patterns, the peak indexed revealed the pure cubic phase of Y_2O_3 . The XRD pattern of $Y_2O_3:Eu^{3+}$ crystals indicates 10 diffraction intense peaks of cubic structure at $2\theta = 20.76, 29.25, 33.96, 36.08, 43.65, 48.63, 53.43, 57.85, 64.66,$ and 78.83 corresponding to (211), (222), (400), (420),

(322), (440), (611), (622), (444), and (662), respectively (Fig. 1). They are in good accordance with JCPDS Card No. 88-1040. This indicated that there is no impurity phase among all the phosphor samples. From these experimental results, we can conclude that Eu^{3+} ions have been introduced into the Y_2O_3 lattice, and did not cause any change in the cubic structure. It was revealed that the introduction of Eu^{3+} ions did not influence the crystal structure of the phosphor matrix. No phase changes were observed when we added different concentrations of Eu^{3+} (0.5–2.5 mol% of Eu). No effect of flux (CaF_2) was found in XRD pattern.

The phosphor particles should have a spherical shape and high luminescence efficiency for successful applications. Indeed, phosphor particles with a spherical shape minimize light scattering on their surfaces and, therefore, improve the efficiency of light emissions and the brightness of such phosphors [40, 41]. To show the evolution particle morphology and size of synthesized $\text{Y}_2\text{O}_3:\text{Eu}^{3+}$ powders, we display in Fig. 2a, b the FEGSEM photographs at two different resolutions. It shows good connectivity with grain size and particle morphology. Here, the solid state method reflects some defects and crack formations in the sample. FEGSEM images represent compact distribution between grains.

Figure 3 shows representative TEM images of Y_2O_3 phosphor doped with 1.5 % of Eu^{3+} ions prepared using the solid state reaction method at 1,300 °C for 4 h. Particles are evidently clustered/aggregated with sizes in the range of 70–90 nm for the 1,300 °C heated sample. The sample has nearly uniform particle size distributions. Selected diffraction patterns showed both dots as well as concentric circles, suggesting the aggregated but nano-crystalline nature of the samples. Average crystallite size observed from XRD pattern (Fig. 1) is found to be smaller compared to that observed from TEM images. This is understandable as the line width of the XRD peak is a measure of the coherent regions present in a particle, whereas TEM images give actual sizes of the particles. From the selected area, the diffraction pattern (SAED) is in good agreement with the XRD pattern.

The phase formation and purity of the products were further confirmed by FTIR spectroscopy, and results are shown in Fig. 4. The strong absorption peak 564 cm^{-1} is ascribed to the stretching vibration of the Y–O bond [42]. The absorption peak at $3,423\text{ cm}^{-1}$ is due to the O–H stretching vibration of H_2O [43]. This is typical of most nanomaterials, since their high specific areas results in significant adsorption of atmospheric water vapor. Like the powder X-ray diffraction (PXRD) results discussed earlier, FT-IR studies further confirm the formation of pure Y_2O_3 product with no other major impurities or secondary phases [44].

Figure 5 shows the excitation (a) and emission (b) spectra of $\text{Y}_2\text{O}_3:\text{Eu}^{3+}$ phosphor sintered at 1,300 °C by the solid state reaction method. The excitation spectra (Fig. 5a) consist of a broad band extending from 200 to 300 nm and some sharp lines in the longer wavelength regions. The former is due to part of the CTB of $\text{Eu}^{3+}-\text{O}^{2-}$ bond, and the latter is from the $f-f$ transitions within the $4f^6$ electron of Eu^{3+} . Upon excitation into the CTB at 254 nm, we obtained the emission spectra.

The emission spectra of $\text{Y}_2\text{O}_3:\text{Eu}^{3+}$ phosphor contain a series of sharp lines in the regions of 400–650 nm, as shown in Fig. 5b. The lines belong to transitions between the energy levels of the $4f^6$ configuration of Eu^{3+} ion [45]. In addition, we can see that there are main emission lines at 582, 594, 615, and 632 nm due to the ${}^5\text{D}_0-{}^7\text{F}_1$,

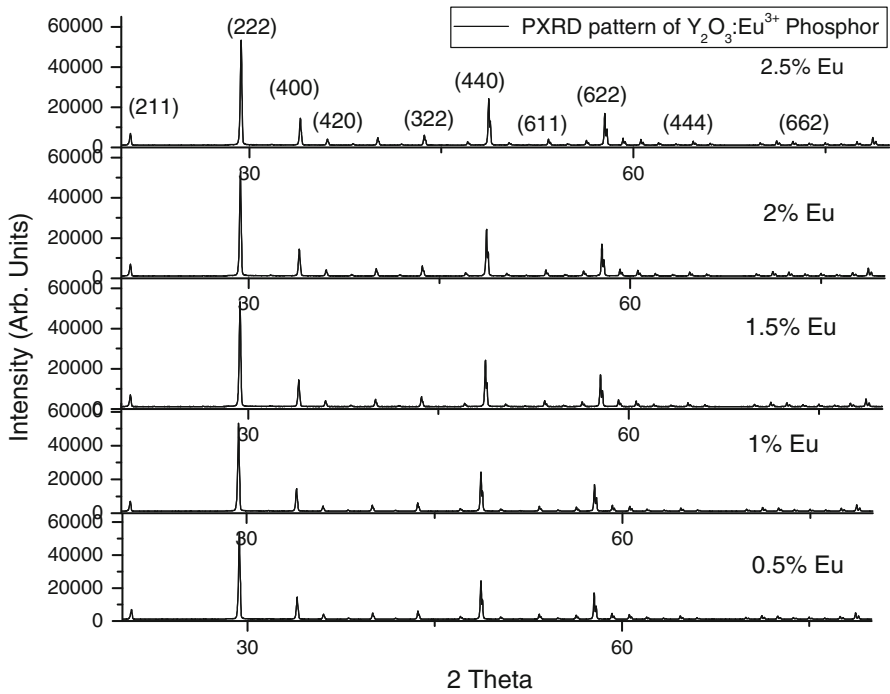


Fig. 1 XRD pattern of $\text{Y}_2\text{O}_3:\text{Eu}$ (0.5–2.5 mol%)

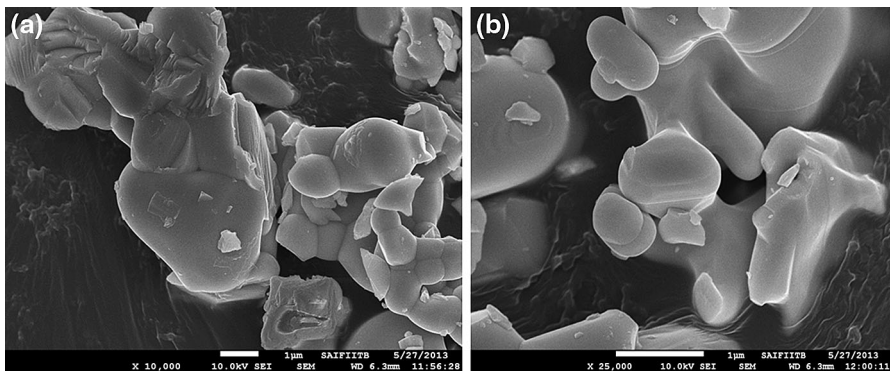


Fig. 2 a, b FEGSEM micrographs of prepared phosphors ($\text{Y}_2\text{O}_3:\text{Eu}^{3+}$ 1.5 mol%)

$^5\text{D}_0\text{--}^7\text{F}_2$, and $^5\text{D}_0\text{--}^7\text{F}_3$ transitions, respectively. The peaks from $^5\text{D}_0$ to $^7\text{F}_2$ (electric-dipole transition) are stronger than those from $^5\text{D}_0\text{--}^7\text{F}_1$ to $^5\text{D}_0\text{--}^7\text{F}_3$ (magnetic-dipole transition). It is known that the $^5\text{D}_0\text{--}^7\text{F}_2$ transition of Eu^{3+} belongs to hypersensitive transitions, which is strongly influenced by the crystal field outside its surroundings. When Eu^{3+} is located at a low-symmetry local site (without an inversion center), this emission transition is often dominated in their emission spectra. Therefore, the Eu^{3+}

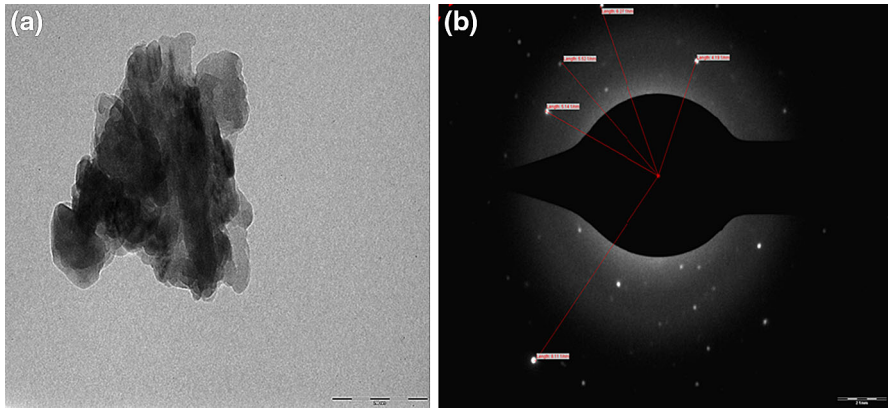


Fig. 3 **a** HRTEM image of prepared phosphor ($\text{Y}_2\text{O}_3:\text{Eu}$ 1.5 mol%), **b** SAED image of prepared phosphor

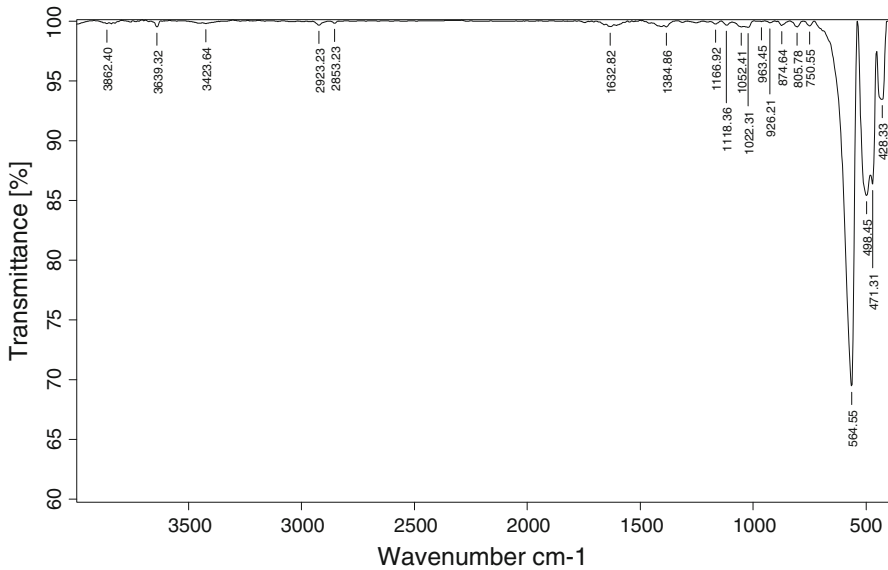


Fig. 4 FTIR spectra of prepared phosphor ($\text{Y}_2\text{O}_3:\text{Eu}$ 1.5 mol%)

ions then occupy on-inversion symmetric Y^{3+} sites [46]. It is well known that Y_2O_3 is a cubic lattice. There are two Y^{3+} sites in cubic Y_2O_3 : 75 % of these sites are non-centro symmetric with C_2 symmetry and the remaining 25 % are centro symmetric having S_6 symmetry [47, 48]. When the Eu^{3+} ion is located at a low-symmetry local site without an inversion center, this forced-electric dipole transition is often dominant in the emission spectrum. So the strongest ${}^5\text{D}_0\text{--}{}^7\text{F}_2$ transition (615 nm) and nearly all of other features in the spectrum are due to the Eu^{3+} on the C_2 site.

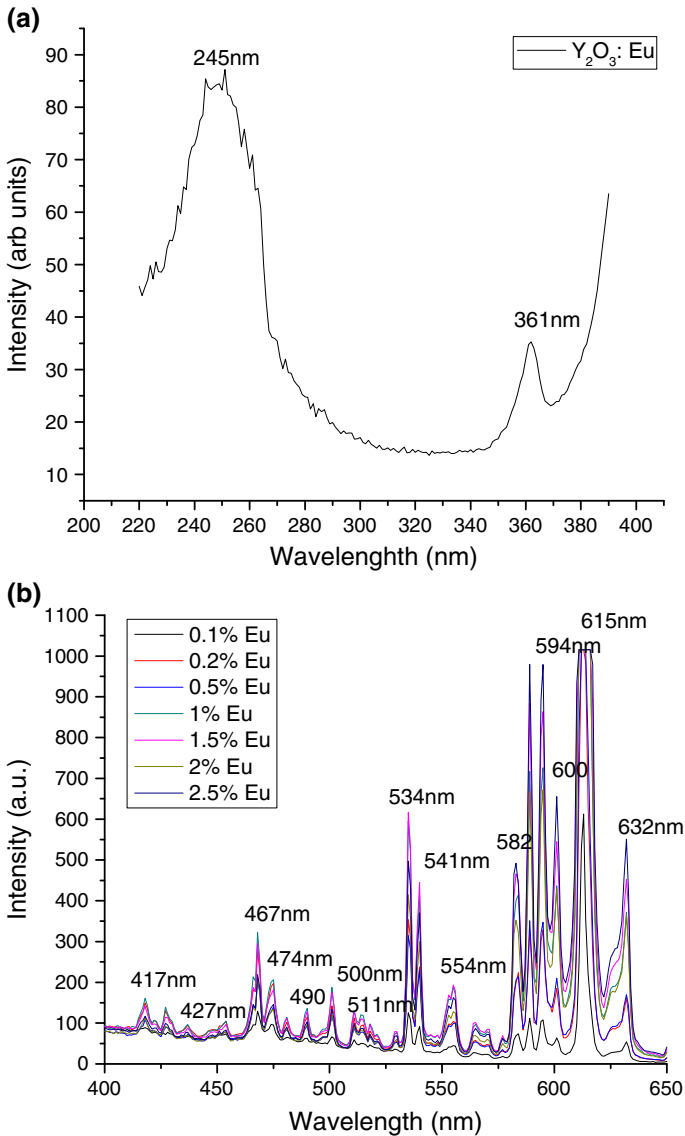


Fig. 5 **a** Excitation spectra of $\text{Y}_2\text{O}_3:\text{Eu}^{3+}$ doped for 400 nm excitation, **b** PL study of $\text{Y}_2\text{O}_3:\text{Eu}^{3+}$ -doped phosphor with variation of Eu^{3+} concentration 254 nm

Figure 5b shows the curve of PL intensity of $\text{Y}_2\text{O}_3:\text{Eu}^{3+}$, which varies with Eu^{3+} mol% (0.1–2.5 %). This picture demonstrates that the best doping value of Eu^{3+} is 1.5 %. The emission band centered at 467 nm is attributed to recombination of a delocalized electron close to the conduction band with a single charged state of surface oxygen vacancy [49]. The emission band at 534 nm can be attributed to self-

trapped excitation luminescence [50]. Other weak emission peaks at 500, 511, 534, and 541 nm are due to different kinds of oxygen vacancies.

Variation in TL intensity with different UV exposures is recorded and shown in Fig. 6a, b, with the variation of different concentrations of Eu^{3+} ion (0.1–2.5 mol%). The peak heights are used for measuring the TL intensities. In Y_2O_3 , TL intensity increases with Eu^{3+} concentration up to 1 mol%, after which it decreases. Possibly, after 1 mol% of Eu^{3+} concentration, quenching occurs and trap levels are destroyed. This trend is generally due to competition between radiative and nonradiative centers, or between different kinds of trapping centers. In the present study, UV exposure is used for creation of defects, and the observed TL glow peaks is mainly attributed to surface defects, since UV radiation cannot penetrate deep into the material [51]. The sublinear increase in TL intensity with UV exposure can be explained on the basis of Horowitz's track interaction model (TIM) [52, 53]. At low exposure times, the recombination of various trapping/luminescent centers (TCs/LCs) occurs entirely within the tracks. Electrons escaping the tracks are intercepted by the non-radiative competitive centers (CC) in the intermediate region.

The TL signal, therefore, linearly increases with the irradiation and is simply proportional to the UV dose (the exposure time) Fig. 7.

TL characterization of the phosphor requires extraction of information regarding trapping parameters such as activation energy (E) of traps, and order of kinetics (b) associated with the glow peaks. Here, E is a measure of energy required to eject an electron from the defect center to the conduction band, while "s" is the rate of electron ejection. The order of kinetics "b" is a measure of the probability that a free electron gets re-trapped. This re-trapping effect increases with density of empty traps. For estimation of trapping parameters (s and E), the following empirical formulae are used to estimate trapping parameters using the Chen's peak shape method [54]:

$$E_\alpha = C_\alpha \left(\frac{k_B T_m^2}{\alpha} \right) - b_\alpha (2T_m), \quad (1)$$

where k_B is Boltzmann constant, and T_m is peak temperature. The constants C_α and b_α were also calculated by the Chen's equation.

Frequency factor (s)

Once E and b are known, the frequency factor (s) can be evaluated:

$$s = \frac{\beta E}{k T_m^2} \exp\left(\frac{E}{k T_m}\right) (1 + (b - 1) \Delta_m^{-1}),$$

where β is the linear heating rate, b the order of kinetics and $\Delta_m = \frac{2kT_m}{E}$.

Order of kinetics

To determine the order of kinetics (b), the form factor or symmetry factor is determined using the following expression:

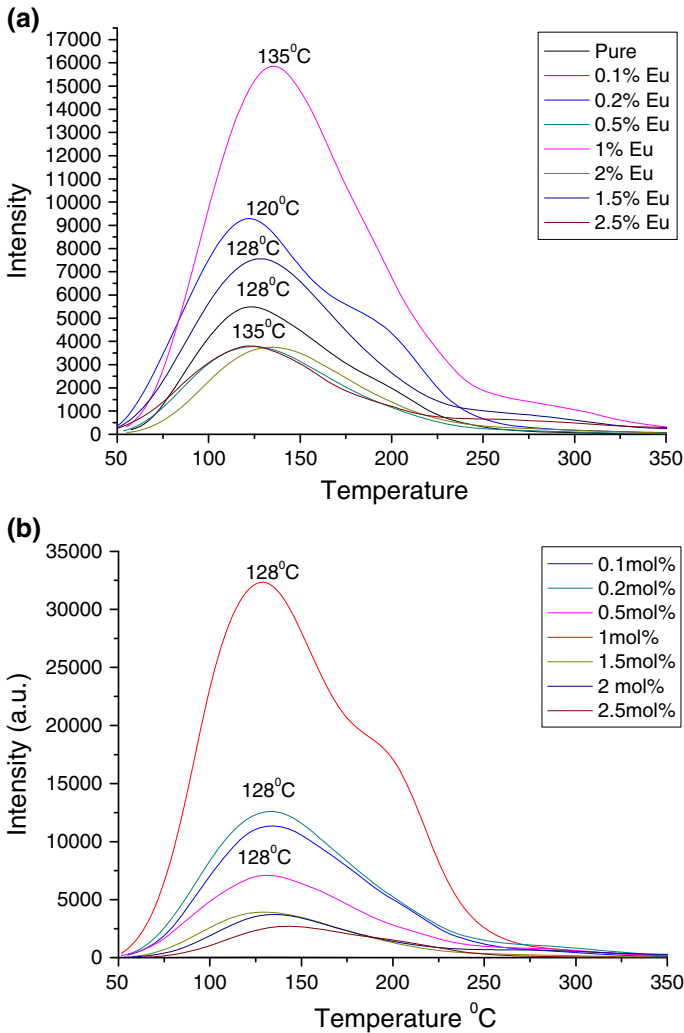


Fig. 6 **a** TL glow curve of Eu-doped Y_2O_3 with the variation of Eu concentration (5 min UV exposure), **b** TL glow curve of Eu-doped Y_2O_3 with the variation of Eu concentration (10 min UV exposure)

$$\mu_g = \frac{T_2 - T_m}{T_2 - T_1}$$

This involves calculation of T_1 and T_2 , which are the temperatures corresponding to half of the maximum intensities on either side of the glow peak maximum temperature (T_m). The nature of the kinetics can be found by the form factor. Theoretically, the value of the geometrical form factor (μ_g) is close to 0.42 for first-order kinetics, and value is 0.52 for second-order kinetics.

The estimated kinetic parameters for $\text{Y}_2\text{O}_3:\text{Eu}^{3+}$ phosphors are given in Tables 1 and 2, respectively.

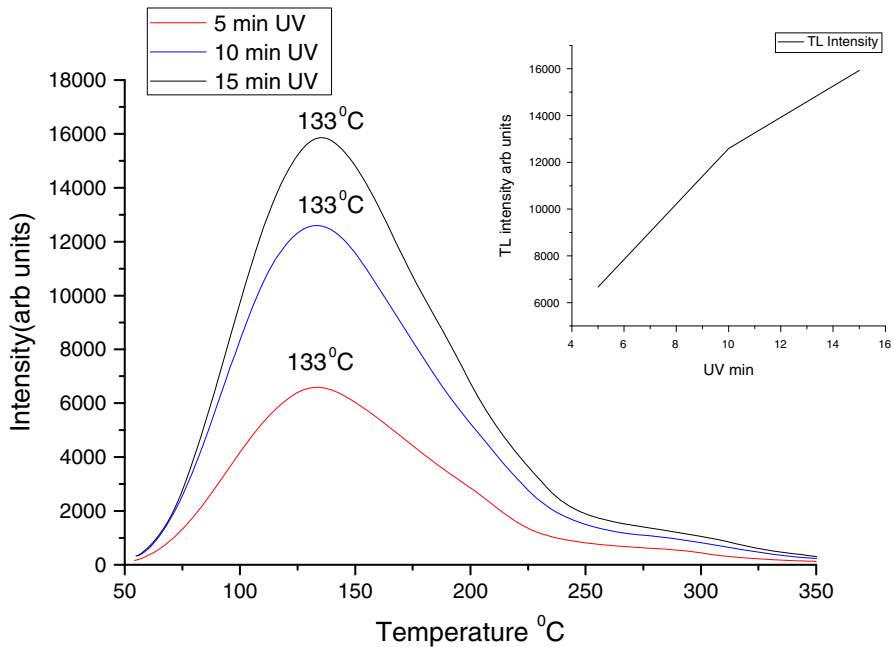


Fig. 7 TL glow curve of $\text{Y}_2\text{O}_3:\text{Eu}$ (1 mol%) with the variation of UV exposure time

Table 1 Shape factors (μ), activation energy (E), and frequency factor (s) for UV-irradiated $\text{Y}_2\text{O}_3:\text{Eu}$ -doped phosphor for 5 min UV

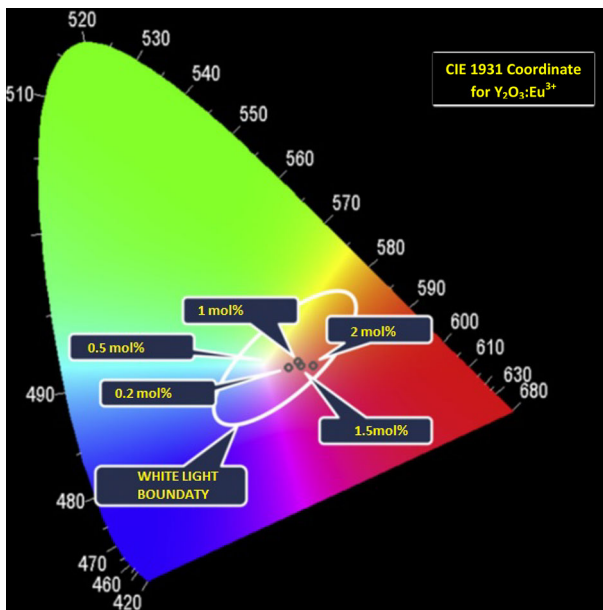
Eu concentration in mol%	T_1	T_m	T_2	τ	δ	ω	$\mu = \delta/\omega$	Activation energy (E)	Frequency factor (s)
0.1	82	135	174	53	39	92	0.42	0.39	5×10^5
0.2	82	120	170	38	50	88	0.56	0.53	9×10^7
0.5	82	135	174	53	39	92	0.42	0.39	5×10^5
1	93	135	189	42	54	96	0.56	0.52	3×10^7
1.5	82	135	174	53	39	92	0.42	0.39	5×10^5
2	87	128	175	41	47	88	0.53	0.51	5×10^7
2.5	82	135	174	53	39	92	0.42	0.39	5×10^5

CIE coordinates

The results indicate that $\text{Y}_2\text{O}_3:\text{Eu}^{3+}$ (1.5 %) phosphors can be selected as a potential candidate for light-emitting diode (LED) applications as well as for FL and compact FL (CFL) (Ex. 254). However, the relative intensity of the emission bands which provide the fundamental color balance for white-light emission was achieved with the 0.5 mol% sample with the spectrum (Fig. 5b) providing the Commission Internationale de l'Éclairage (CIE) 1931 chromaticity coordinates much closer to the equal-energy white light (Fig. 8). If one increases the activator concentration even further, the emission intensity starts to decrease owing to concentration quenching, which is due to the

Table 2 Shape factors (μ), activation energy (E) and frequency factor (s) for UV-irradiated $Y_2O_3:Eu$ -doped phosphor for 10 min UV

Eu concentration in mol%	T_1	T_m	T_2	τ	δ	ω	$\mu = \delta/\omega$	Activation energy (E)	Frequency factor (s)
0.1	95	131	175	36	44	80	0.55	0.59	3×10^8
0.2	93	128	182	35	54	89	0.60	0.61	8×10^8
0.5	90	128	179	38	51	89	0.57	0.56	1×10^8
1	89	128	194	39	66	105	0.62	0.56	1×10^8
1.5	90	128	176	38	48	86	0.55	0.55	1×10^8
2	90	128	178	38	50	88	0.56	0.56	2×10^8
2.5	92	128	177	36	49	85	0.57	0.59	3×10^8

**Fig. 8** CIE coordinates depicted on 1,931 chart of Eu (0.2–2 %)-doped Y_2O_3 phosphor

increase in the ion–ion interaction provoked by the shorter distance between interacting activators as the concentration increases. The fluorescence light spectral profile as a function of the activator concentration was examined and the results indicated that the chromaticity coordinates of the overall emission light changed, resulting in different colors of the overall emission light for different concentrations, as can be observed.

Conclusion

$Y_2O_3:Eu^{3+}$ -doped phosphor synthesized by the solid state reaction method. XRD pattern confirms that the synthesized sample shows a cubic structure. The crystallite

size was found to be in the range of 70–90 nm. XRD studies confirm that the phosphors are in single phase and nano-crystallites. FEGSEM images show the formation of nano-spheres. It can be seen that the particles have a compact distribution and spherical shape. The PL emission was observed in the range 417–632 nm for all visible regions for the Y_2O_3 phosphor doped with Eu^{3+} . The excitation spectrum was found at 254 nm. Sharp intense peaks were found around 467, 534, 594, 612, and 632 nm with high intensity. The present phosphor can act as a single host for white light emission in display devices. The results indicate that $Y_2O_3:Eu^{3+}$ (1.5 %) phosphors can be selected as potential candidates for LED application as well as for FL and CFL (Ex. 254).

The TL kinetic parameters are also calculated using the glow curve shape method. The results indicate that the TL glow curves of samples follow a second-order kinetic model. The observed PL is due to oxygen deficiencies in the Y_2O_3 , while the observed TL characteristics (e.g., supra-linearity in the intensity variation with dosage) is understood using TIM. Corresponding activation energy was found in between 0.39 and 0.61 eV and the frequency factor is 5×10^5 – 8×10^8 s⁻¹.

References

1. R. Reisfeld, K. Jorgensen, *Lasers and Excited states of Rare Earths* (Springer, New York, 1978)
2. E. Antic-Fidancev, J. Holsa, M. Lastusaari, J. Alloys Compd. **341**, 82 (2002)
3. T. Jüstel, J.C. Krupa, D.U. Wiechert, J. Lumin. **93**, 179 (2001)
4. X. Peng, L. Manna, W. Yang, J. Wickham, E. Scher, A. Kadavanich, A.P. Alivisatos, Nature **404**, 59 (2000)
5. L. Fornasiero, E. Mix, V. Peters, K. Petermann, G. Huber, Ceram. Int. **26**, 589 (2000)
6. H. Eilers, B.M. Tissue, Chem. Phys. Lett. **251**, 74 (1996)
7. M. Kottaiswamy, D. Jeyakumar, R. Jagannathan, M. Mohan Rao, Mater. Res. Bull. **31**, 1013 (1996)
8. B. Bihari, H. Eilers, B.M. Tissue, J. Lumin. **75**, 1 (1997)
9. T. Ye, Z. Guiwen, Z. Weiping, X. Shangda, Mater. Res. Bull. **32**, 501 (1997)
10. F. Wang, Y. Han, C.S. Lim, Y. Lu, J. Wang, J. Xu, H. Chen, C. Zhang, M. Hong, X. Liu, Nature **463**, 1061–1065 (2010)
11. R.D. Shannon, Acta Crystallogr. Sect. A **32**, 751–767 (1976)
12. M. Maestro, D. Huguenin, A. Seigneurin, F. Deneuve et al., J. Electrochem. Soc. **139**(5), 1479 (1992)
13. X.R. Hou, S.M. Zhou, H. Lin, H. Teng, Y.K. Li, W.J. Li, T.T. Jia, J. Appl. Phys. **107**(8), 083101 (2010)
14. L.O.O. Costa, A.M. Silva, L.E.P. Borges, L.V. Mattos, F.B. Noronha, Catal. Today **138**(3–4), 147 (2008)
15. A.M. Edwin Suresh Raj, C. Maria Magdalane, K.S. Nagaraja, Phys. Status Solid **191**(1), 230 (2002)
16. G.K. Das, T.T.Y. Tan, J. Phys. Chem. C **112**(30), 11211 (2008)
17. Y.L. Kopylov, V.B. Kravchenko, A.A. Komarov, Z.M. Lebedeva, V.V. Shemet, Opt. Mater. **29**(10), 1236 (2007)
18. W.J. Li, S.M. Zhou, H. Lin, H. Teng, N. Liu, Y.K. Li, X.R. Hou, T.T. Jia, J. Am. Ceram. Soc. **93**(11), 3819 (2010)
19. A. Fukabori, T. Yanagida, J. Pejchal, S. Maeo, Y. Yokota, A. Yoshikawa, T. Ikegami, F. Moretti, K. Kamada, J. Appl. Phys. **107**(7), 073501 (2010)
20. C. Burda, X.B. Chen, R. Narayanan, M.A. El-Sayed, Chem. Rev. **105**(4), 1025 (2005)
21. X.Y. Ye, W.D. Zhuang, Y.S. Hu, T. He, X.W. Huang, C.F. Liao, S.W. Zhong, Z.F. Xu, H.P. Nie, G.F. Deng, J. Appl. Phys. **105**(6), 064302 (2009)
22. G.S. Wu, Y. Lin, X.Y. Yuan, T. Xie, B.C. Cheng, L.D. Zhang, Nanotechnology **15**(5), 568 (2004)

23. Y.B. Mao, T. Tran, X. Guo, J.Y. Huang, C.K. Shih, K.L. Wang, J.P. Chang, *Adv. Funct. Mater.* **19**(5), 748 (2009)
24. S. Sohn, Y. Kwon, Y. Kim, D. Kim, *Powder Technol.* **142**(2–3), 136 (2004)
25. X. Bai, H.W. Song, L.X. Yu, L.M. Yang, Z.X. Liu, G.H. Pan, S.Z. Lu, X.G. Ren, Y.Q. Lei, L.B. Fan, *J. Phys. Chem. B* **109**(32), 15236 (2005)
26. N. Zhang, X.H. Liu, R. Yi, R.R. Shi, G.H. Gao, G.Z. Qiu, *J. Phys. Chem. C* **112**(46), 17788 (2008)
27. S.Y. Zeng, K.B. Tang, T.W. Li, Z.H. Liang, *J. Colloid Interface Sci.* **316**(2), 921 (2007)
28. H.Z. Wang, M. Uehara, H. Nakamura, M. Miyazaki, H. Maeda, *Adv. Mater.* **17**(20), 2506 (2005)
29. J.H. Jeong, B.K. Moon, H.J. Seo, J.S. Bae, S.S. Yi, I.W. Kim, H.L. Park, *Appl. Phys. Lett.* **83**, 1346 (2003)
30. T.W. Kelley, A.L. Diaz, T.A. Dang, *Chem. Mater.* **18**, 3130 (2006)
31. J.Y. Zhang, Z.L. Tang, *Mater. Sci. Eng. A* **334**, 246 (2002)
32. O.A. Serra, S.A. Cicillini, R.R. Ishiki, *J. Alloy. Compd.* **303–304**, 316 (2000)
33. N. Salah, S.S. Habib, Z.H. Khan, S. Al-Hamed, S.P. Lochab, *J. Lumin.* **129**, 192 (2009)
34. P.J.R. Montes, M.E.G. Valerio, M.A. Macedo, F. Cunha, J.M. Sasaki, *Microelectron. J.* **34**, 557 (2003)
35. V. Dubey, J. Kaur, S. Agrawal, *Res. Chem. Intermed.* (2013). doi:[10.1007/s11164-013-1201-5](https://doi.org/10.1007/s11164-013-1201-5)
36. V. Dubey, J. Kaur, S. Agrawal, N.S. Suryanarayana, K.V.R. Murthy, *J. Light Electron Opt.* (2013). doi:[10.1016/j.ijleo.2013.03.153](https://doi.org/10.1016/j.ijleo.2013.03.153)
37. V. Dubey, N.S. Suryanarayana, J. Kaur, Kinetics of TL glow peak of limestone from Patharia of CG Basin (India). *J. Miner. Mater. Charac. Eng.* **9**(12), 1101–1111 (2010)
38. V. Dubey, J. Kaur, N.S. Suryanarayana, K.V.R. Murthy, *Res. Chem. Intermed.* (2012). doi:[10.1007/s11164-012-0872-7](https://doi.org/10.1007/s11164-012-0872-7)
39. V. Dubey, J. Kaur, S. Agrawal, N.S. Suryanarayana, K.V.R. Murthy, *Superlattices Microstruct.* **67**, 156–171 (2014)
40. M.K. Devaraju, S. Yin, T. Sato, *J. Cryst. Growth* **311**, 580 (2009)
41. A. Boukerika, L. Guerbous, *J. Lumin.* **145**, 148–153 (2014)
42. S. Som, S.K. Sharma, *J. Phys. D* **45**, 415102–415108 (2012)
43. H. Qin, H. Liu, Y. Sang, Y. Lv, X. Zhang, Y. Zhang, T. Ohachi, J. Wang, *Cryst. Eng. Comm.* **14**, 1783–1789 (2012)
44. R. Hari Krishna, B.M. Nagabhushana, H. Nagabhushana, R.P.S. Chakradhar, R. Sivaramakrishna, C. Shivakumara, T. Tiju, *J. Alloy. Compd.* **585**, 129–137 (2014)
45. J. Yang, Z.W. Quan, D.Y. Kong, X.M. Liu, J. Lin, *Cryst. Growth Des.* **7**, 730 (2007)
46. D. Ravichandran, R. Roy, A.G. Chakhovskoi, C.E. Hunt, W.B. White, S. Erdei, *J. Lumin.* **71**, 291 (1997)
47. J. Silver, M.I. Martinez, T.G. Ireland, R.J. Withnall, *J. Phys. Chem. B* **105**, 7200 (2001)
48. M. Maitric, B. Antic, M. Balanda, D. Rodic, M.L. Napijalo, *J. Phys.* **9**, 4103 (1997)
49. C. Hu, H. Liu, W. Dong, Y. Zhang, G. Bao, C. Lao, Z.L. Wang, *Adv. Mater.* **19**, 470–474 (2007)
50. Y. Zhang, K. Han, T. Cheng, Z. Fang, *Inorg. Chem.* **46**, 4713–4717 (2007)
51. M. Chandrasekhar, D.V. Sunitha, N. Dhananjaya, H. Nagabhushana, S.C. Sharma, B.M. Nagabhushana, C. Shivakumara, R.P.S. Chakradhar, *J. Lumin.* **132**, 1798–1806 (2012)
52. Y.S. Horowitz, O. Avila, M. Rodriguez-Villafuerte, *Nucl. Instr. Method. Phys. Res. B* **184**, 85–112 (2001)
53. Y.S. Horowitz, M. Rosenkrantz, S. Mahajana, D. Yosian, *J. Phys. D* **9**, 205–211 (1995)
54. R. Chen, Y. Kirish, *Analysis of Thermally Stimulated Processes* (Pergamon, New York, 1981)